Journal of Power Sources 260 (2014) 50–56

Contents lists available at ScienceDirect

Journal of Power Sources

journal homepage: www.elsevier.com/locate/jpowsour

Capacity fading of $LiAl_yNi_{1-x-y}Co_xO_2$ cathode for lithium-ion batteries during accelerated calendar and cycle life tests (effect of depth of discharge in charge–discharge cycling on the suppression of the micro-crack generation of $LiAl_yNi_{1-x-y}Co_xO_2$ particle)

Shoichiro Watanabe [a,*], Masahiro Kinoshita [b], Takashi Hosokawa [c], Kenichi Morigaki [a], Kensuke Nakura [b]

[a] Portable Rechargeable Battery Business Division, SANYO Electric Co., Ltd, Automotive & Industrial Systems Company of Panasonic Group, 139-32, Toyohisa, Matsushige-Cho, Itano-gun, Tokushima 771-0213, Japan
[b] Device Solution Center, Panasonic Corporation, 1006 Kadoma, Kadoma City, Osaka 571-8501, Japan
[c] Automotive Battery Business Division, SANYO Electric. Co., Ltd., Automotive & Industrial Systems Company of Panasonic Group, 194-4, Tokonabe-cho, Kasai City, Hyogo 675-2332, Japan

HIGHLIGHTS

- We investigate the degradation of Li-ion cell during cycle with ΔDOD restriction.
- Many micro cracks were observed only after a 0–100% DOD region cycle test.
- The deterioration was not closely related to the upper and lower limits of DOD.

ARTICLE INFO

Article history:
Received 28 October 2013
Received in revised form
6 January 2014
Accepted 27 February 2014
Available online 12 March 2014

Keywords:
Deterioration
Cycle performance
Micro-crack
Lithium nickel cobalt aluminum oxide
Lithium-ion batteries

ABSTRACT

Cycle performance of a $LiAl_{0.10}Ni_{0.76}Co_{0.14}O_2$ (NCA) cathode/graphite cell closely depended on the range of depth of discharge in charge–discharge processes (ΔDOD). When ΔDOD was 10–70%, cycle performance at 25 °C was maintained even at 60 °C. Deterioration phenomena were analyzed by electrochemical method, X-ray photoelectron spectroscopy (XPS), X-ray diffractometry (XRD), and micro-cracks in NCA particles were analyzed with cross-sectional views by scanning electron microscopy (SEM). Many micro-cracks were observed only after a 0–100% DOD region cycle test. Cycle tests in several restricted ΔDOD conditions showed that the deterioration was closely related to not the upper and lower limits of DOD or operation voltage but the width of ΔDOD.

1. Introduction

The high power storage system composed of multi-cylindrical lithium-ion batteries (LIBs) was proposed for the EV power supply and the household electric energy storage applications. In this system 18650-standard size cylindrical LIBs are used because they have high energy density and comparatively lower cost [1]. A Ni-based $LiAl_yNi_{(1-x-y)}Co_xO_2$ cathode active material for cylindrical LIBs is the most promising one in high energy density storage applications because of its high capacity and cost/storage Wh performance [2–10]. There have been a number of investigations to improve the storage and cycle performance with doping several species into cathode active materials. The addition of aluminum improves cycle life, thermal stability at charged states and cathodic overpotential [9,11–14].

Panasonic has launched the NCR18650 series lithium-ion batteries with the $LiAl_yNi_{(1-x-y)}Co_xO_2$ cathode into the market since 2006. They have high energy density of 620 Wh dm^{-3} for a 18650-type 10 Wh cylindrical cell and good storage performance. Recently, Panasonic has commercialized 12 Wh lithium-ion batteries

* Corresponding author. Tel.: +81 88 699 9395; fax: +81 88 699 9046.
E-mail address: watanabe.sho-ichiro@jp.panasonic.com (S. Watanabe).

http://dx.doi.org/10.1016/j.jpowsour.2014.02.103
0378-7753/

(725 Wh dm^{-3}) which is the highest energy density in commercially available LIBs. The LIBs with $LiAl_yNi_{(1-x-y)}Co_xO_2$ cathode show much longer storage calendar life than conventional batteries with cobalt-based oxide cathodes [18,19], and they started to be used not only for mobile phones but also for electric storage systems and the vehicle power supplies.

Longer calendar and cycle lives are required for the high power applications compared to the conventional mobile usage. Batteries are stored at high states of charge (SOCs), and repetitively charged and discharged in wide ranges of depth of discharge (DOD). Broussely et al. investigated long-term stability of the LIBs with the Ni-based oxide cathode for satellite or standby applications, and found they exhibited outstanding stability on cycling and storage [15–17].

On the other hand, when the LIBs with $LiAl_yNi_{(1-x-y)}Co_xO_2$ cathode were subjected to charge–discharge cycle tests in large ΔDOD conditions at high temperatures such as 40–70 °C, serious capacity fading and power loss due to the increase in impedance at the cathode/electrolyte interface have been reported [20–24]. Aluminum doping was found very effective to suppress the cell impedance rise by stabilizing the charge-transfer on the cathode side [25–29]. Moreover, it was reported that cycle characteristics remarkably depended on ΔDOD [30]. The ΔDOD influenced the capacity fading and power loss in $LiAl_yNi_{(1-x-y)}Co_xO_2$/Graphite cells. From a comparison between cells cycled in ΔDOD conditions of 0–100% and 0–70%, the capacity of the former faded much faster than that of the latter.

Ukyo et al. reported that the morphology of $LiAl_{0.05}Ni_{0.8}Co_{0.15}O_2$ particles changed during charge–discharge cycling at 60 °C [31,32]. They suggested that the growth of micro-cracks formed at grain boundaries of the $LiAl_yNi_{(1-x-y)}Co_xO_2$ particles as spherical secondary ones which consist of small primary particles was responsible for the increase in cell resistance because of the interruption of electronic and ionic conduction. Moreover, they showed the surface of the micro-cracks turned from an ordered layer structure (α-$NaFeO_2$-type) to a partially ordered structure and then to a disordered rock-salt structure during the first charge–discharge cycle [33,34]. ΔDOD and temperature also induced the increase in cell resistance. However, it has not been elucidated why the larger ΔDOD accelerated increase in cell resistance. In this regard, there are two possibilities: (1) Deterioration of active materials occurred in a specific potential region, (2) Crystal structure of active materials was destroyed in larger ΔDOD conditions. It is significant to clarify the reason for improving battery performance. Recently, we have reported that cylindrical LIBs with the NCA cathode had outstanding cycle performance in charge–discharge cycle tests in which ΔDOD was restricted [35,36]. In this study, the effect of micro-cracks on battery performance, in particular cell resistance, of the LIBs with the NCA cathode was investigated by charge–discharge tests in various ΔDOD conditions.

2. Experimental

2.1. Cycle tests in different ΔDOD conditions for cylindrical model cells

A cylindrical model cell with capacity of 400 mAh which was composed of a lithium nickel cobalt aluminum oxide cathode which consisted of a mixture of NCA, carbon black and poly vinylidene fluoride, a graphite anode, electrolyte and a microporous polyethylene separator was used in this investigation. Electrolyte was a mixture of ethylene carbonate (EC), ethyl methyl carbonate (EMC), and dimethyl carbonate (DMC) with lithium hexafluorophosphate ($LiPF_6$).

Charge–discharge cycle tests were executed by two series. First series were performed with two ΔDOD conditions (DOD 0–100% and DOD 10–70%) at 25 and 60 °C. These tests were operated at a current rate of 1C (400 mA). Capacity checking test was performed at every 50 cycles during 0–500 cycles and at every 500 cycles during 500–2500 cycles to compare discharge capacity in the voltage region of 4.2–2.5 V among four conditions.

Second series were performed at 25 °C in four ΔDODs which were 0–60% (4.2–3.54 V), 10–70% (4.05–3.48 V), 40–100% (3.78–2.5 V) and 0–100%. The charge–discharge cycle tests were operated at a current rate of 2C (800 mA). The charge condition was CC–CV, and CV cut current value was 0.05C (20 mA). Discharge capacity checking test was performed in the voltage region of 4.2–2.5 V at every 500 cycles. The detail test conditions are summarized in Table 1.

2.2. Impedance analysis of coin-type model cells

In order to investigate the increase in impedance and capacity deteriorations for the cathode and anode, cylindrical cells were disassembled to remove the cathode and anode, and each was rinsed by DMC, and then used to assemble a coin-type cell with a Li metal as a counter electrode under dry air atmosphere. The deterioration capacity was measured by charge–discharge tests and compared with a fresh electrode. The change in cell impedance was measured by a Solartron 1260/1286 frequency response analyzer system.

2.3. Surface and bulk analyses

X-ray diffraction (XRD) patterns were collected with a Panalytical X'Celerator detector equipped with a Cu target x-ray tube and a diffracted beam monochromator. Each XRD measurement was performed every 0.05° over a scattering angle region between $2\theta = 10$ and 90° and the counting time was 10 s. Rietveld refinement was performed by using HighScore (plus) software package. Scanning electron microscopy (SEM) was carried out to observe a cross section of an NCA particle after being treated by cross section polisher. SEM images were taken with a scanning electron microscope Hitachi S-4500 equipped with an energy-dispersive X-ray (EDX) analyzer.

Table 1
The charge–discharge cycle test conditions of 18650 cells.

Cycle test	Charge	CCCV; charged at 1.0 C rate up to (a) 4.2 V and (b) 4.05 V 0.05 C-cutoff
	Charge rest	20 min
	Discharge	1.0 C rate, (a) 2.5 V and (b) 3.48 V-cutoff
	Discharge rest	20 min
Capacity check	Charge	CCCV; charged at 1.0 C rate up to 4.2 V 0.05 C-cutoff
	Charge rest	20 min
	Discharge	1.0 C rate, 2.5 V-cutoff
	Discharge rest	20 min
Cycle test	Charge	CCCV; charged at 2.0 C rate up to (a) 4.2 V (b) 4.05 V (c) 3.78 V and (d) 4.2 V 0.05 C-cutoff
	Charge rest	20 min
	Discharge	1.0 C rate, (a) 3.54 V (b) 3.48 V (c) 2.5 V (d) 2.5 V-cutoff
	Discharge rest	20 min
Capacity check	Charge	CCCV; charged at 1.0 C rate up to 4.2 V 0.05 C-cutoff
	Charge rest	20 min
	Discharge	1.0 C rate, 2.5 V-cutoff
	Discharge rest	20 min

XRD and SEM were used to study the phase change and microscopic morphology for active materials after cycling. For surface and bulk analyses, each cell was discharged to a voltage of 2.5 V at 1 C rate and then disassembled. The samples taken out of the disassembled cells were washed with dry DMC and evaporated at room temperature. Other experimental conditions are given in the next section.

3. Results and discussion

3.1. Cycle performance of cylindrical mode cells in the different ΔDOD conditions and characteristics of disassembled cathodes

Fig. 1 shows charge–discharge cycle performance for NCA cathode/graphite anode cylindrical model cells in two ΔDOD conditions at 25 and 60 °C. The vertical axis of relative capacity is defined as the ratio of discharge capacity at a certain cycle to the initial one. In the ΔDOD condition of 0–100%, significant capacity fading was observed, and the capacity was deteriorated more rapidly at higher temperature. On the other hand, in the ΔDOD condition of 10–70%, cycle performance was greatly improved even at 60 °C. These results indicated that the mechanism for capacity deterioration of LIBs with the NCA cathode was not simple. Furthermore, in the program of the advanced technology development (ATD), Lithium ion cells with NCA cathode were pulse-tested at high temperature with a high-power profile but only with a very narrow range of variation of ΔDOD such as 3% and 6%. The capacity of these cells was found to be stable and the large increases in cell impedance with both cycling and aging [22–24]. The capacity fading mechanism in the ΔDOD condition of 0–100% was not same as narrow range ΔDOD cycling.

The NCA cathode or graphite anode after cycle tests was reassembled into 2016 type coin cells with Li metal as a counter electrode. Cell impedance for each coin-type cell is shown in Fig. 2. The cell impedance was measured at 70% DOD and 25 °C and the resistance was evaluated from the low frequency semicircle in each Nyquist plot. The resistance value of NCA cathode at initial state was 14.07 Ω and the values after 10–70% DOD cycle test were 11.03 Ω at 25 °C and 21.30Ω at 60 °C, respectively, while the value after 0–100% DOD cycle test was 230.80 Ω at 60 °C. From the results, the resistance value was significantly increased only for the cell with the NCA cathode after 0–100% DOD cycle test, while the resistance change was not observed for the cells with the NCA cathode after 10–70% DOD cycle test. As for the cell with the graphite anode, the resistance was almost equal irrespective of ΔDOD cycle test condition and operating temperature. The results of impedance analysis for cathode and anode in the ΔDOD condition of 0–100% were corresponding to the result of previous investigations [20,28,29]. Zhang et al. showed that the resistance in equivalent circuit is composed of Ohmic (R_{ohm}), Charge transfer (R_{ct}) and resistance of SEI layer (R_{SEI}), and the dominant resistance of increasing the impedance is R_{SEI} [29]. Therefore, in this study, we assume that the increase of the resistance of low frequency semicircle in the ΔDOD of 0–100% must be R_{SEI}. The surface structure change will be analyzed in further literature by XPS and TEM-EELS. On the other hand, the reason of the increase of R_{SEI} after 0–100% ΔDOD cycle test was not clarified.

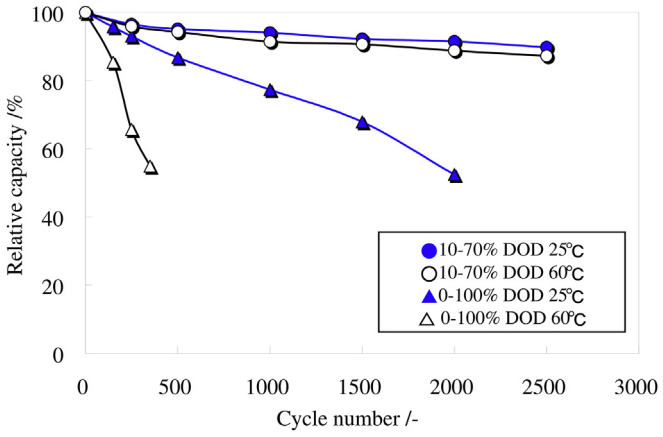

Fig. 1. Cycle performance of NCA cathode/graphite anode model cells in two ΔDOD conditions at 25 and 60 °C; (●) 10–70% DOD at 25 °C, (○) 10–70% DOD at 60 °C, (▲) 0–100% DOD at 25 °C and (△) 0–100% DOD at 60 °C.

Fig. 3 shows discharge curves of the reassembled coin-type cells operated in a voltage region of 4.3–2.5 V for NCA cathode or of 1.0–0.01 V for graphite anode at a constant current of 0.1C at 25 and 60 °C. After cycle tests in the ΔDOD of 0–100%, capacity loss for the cell with the NCA cathode was 33.5% at 25 °C and 45.2% at 60 °C, while that for the cell with the graphite anode was about 10%. These results suggest that the capacity loss is mainly ascribed to the deterioration of the NCA cathode which is influenced by ΔDOD cycle test condition and temperature. On the other hand, after cycle tests in the ΔDOD of 10–70%, capacity loss for the cell with the NCA cathode was 1.5% at 25 °C and 9.9% at 60 °C, These results indicate that the capacity loss is strongly affected by ΔDOD cycle test condition and test temperature.

In order to investigate the cause of deterioration of the NCA cathode accelerated by cell tests in the ΔDOD of 0–100% at 25 and 60 °C, the cathode and anode disassembled before and after cycle tests were characterized by XRD and SEM. Fig. 4 shows XRD patterns of the NCA cathode before and after cycle tests. Neither new diffraction peaks nor significant peak shift were observed after cycle tests, suggesting that crystal structure of NCA bulk did not suffer serious damage during cycle tests, suggesting that this is not the cause of capacity loss. Shim et al. and Striebel et al. studied XRD, Raman and CSAFM for deteriorated cathode after cycling in the ΔDOD of 0–100% at 60 °C. The results of XRD were almost same as this study, and they suggested capacity loss occurs due to a rise in the impedance of the cathode caused by loss of the conductive carbon at the surface and/or by an organic film on the surface of the cathode [25,30]. Therefore, we investigated the detail analysis for the cathode surface and bulk structure.

3.2. Change in morphology and electrochemical properties of $LiAl_yNi_{(1-x-y)}Co_xO_2$ particles with charge–discharge cycling in different ΔDOD conditions and temperatures

Fig. 5 shows cross sectional SEM images (image a–e) of NCA particles before and after cycle tests. After each cycle test, micro-cracks in NCA particles were remarkably observed after 2000 cycles at 25 °C and 350 cycles at 60 °C in the ΔDOD of 0–100%. In order to quantify the micro-crack generation, each SEM image were converted to black areas due to micro-cracks and original pores and white ones due to NCA domains by image processing (image f–j), and then area ratio of black to white was calculated and given in converted images. It was revealed that the micro-crack generation was accelerated at 60 °C in the ΔDOD of 0–100%, while in the ΔDOD of 10–70% it was small even at 60 °C and there was little difference in black/white area ratio between 25 and 60 °C. These results indicate that the micro-crack generation in the NCA particles is one of the main deterioration factors of NCA cathode.

The BET surface area of the NCA cathode before and after cycle tests is also shown in Fig. 5. When the cells were cycled in the ΔDOD condition of 0–100%, BET surface area has increased by 100% or more because of the increase in initial surface to contact with

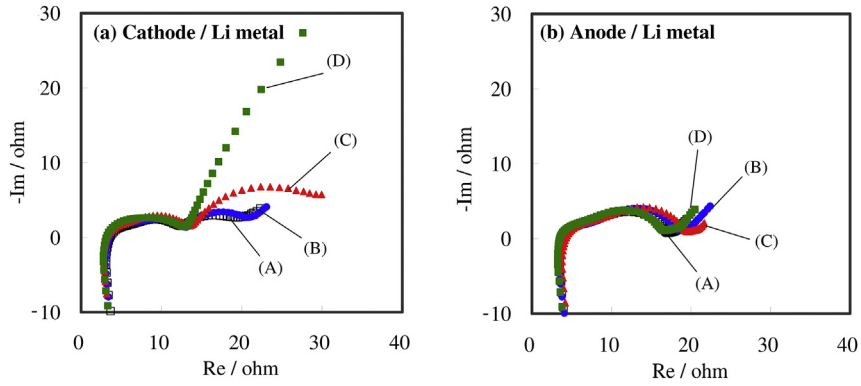

Fig. 2. Nyquist plots of coin cells before and after cycle tests; (a) NCA cathode/Li metal cell (A) initial, (B) 10–70% DOD at 25 °C, 2500 cycles, (C) 10–70% DOD at 60 °C, 2500 cycles, (D) 0–100% DOD at 60 °C, 350 cycles, (b) Graphite anode/Li metal cell (A) initial, (B) 10–70% DOD at 25 °C, 2500 cycles, (C) 10–70% DOD at 60 °C, 2500 cycles, (D) 0–100% DOD at 60 °C, 350 cycles.

infiltrated electrolyte along the micro-cracks. Ukyo et al. studied the formation of micro-crack was observed even in after first cycle. They found the structure at micro-crack surface gradually changed from an ordered layer structure (α-$NaFeO_2$-type) to a partially ordered structure and then to a disordered rock-salt structure [33,34]. It was thought that not only the declining of electronic conduction by generation of micro-crack, but the new disordered layer could be formed on the initial surface of the grain boundary, which would increase the impedance of the cathode. The viscosity of electrolyte decreased from 0.023 P at 25 °C to 0.012 P at 60 °C. It was suggested that the acceleration of electrolyte infiltration to the cleft of microcrack caused the deterioration at high temperature.

The results of deterioration phenomena of $LiAl_{0.10}Ni_{0.74}Co_{0.16}O_2$ cathode are corresponding to previous investigation with $LiAl_{0.05}Ni_{0.8}Co_{0.15}O_2$ cathode of cycling in the ΔDOD of 0–100% by Striebel et al. and Ukyo et al. [30,31]. However, reason of the different cycling characteristics in the ΔDOD 0–100% compared with the case of ΔDOD 10–70% has not explained by the proposed deterioration mechanism. Ukyo et al. studied the relationship between the increase of resistance and potential window during cycling. The increase in resistance was reduced with decrease of the potential window. (For example, 154 mAh g^{-1} between 4.1 V and 2.5 V to 98 mAh g^{-1} between 4.1 V and 3.0 V) It was thought that the volume change of positive material caused the increase in resistance. On the other hand, they showed the many cracks were formed by charged at $x = 0.6$ in $Li_{1-x}Al_{0.05}Ni_{0.8}Co_{0.15}O_2$ which was the distortion point of the crystal lattice. The effect of cycling with crystal distortion point have not examined yet because of the control of the charge voltage until at 4.1 V in previous studies [30,31]. The reason of the different cycling characteristics in the ΔDOD 0–100% compared with that in ΔDOD condition of 10–70% estimated two possibilities: (1) Deterioration of active materials occurred in a specific potential region, (2) Crystal structure of active materials was destroyed in larger ΔDOD conditions. Therefore, we

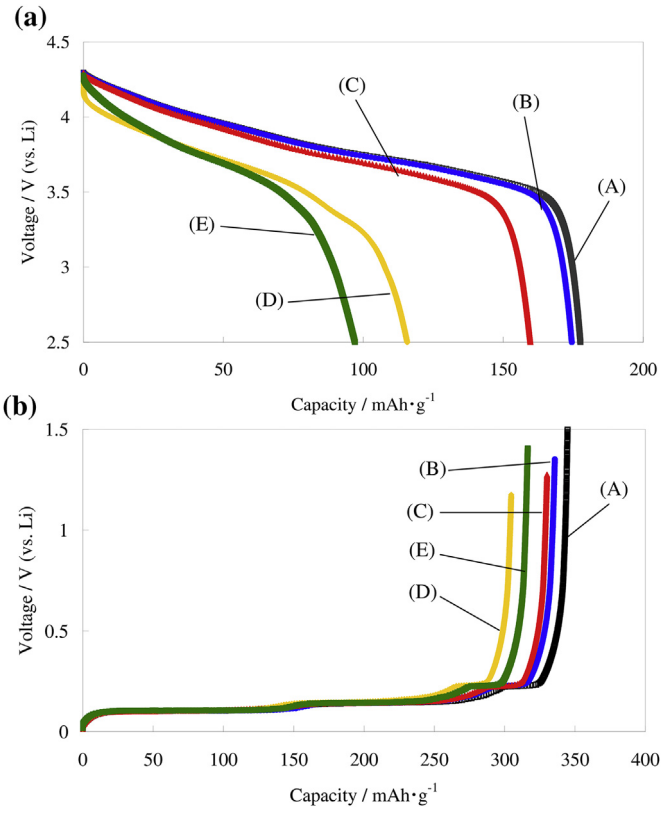

Fig. 3. Discharge curves of the cells with (a) NCA cathode electrode and (b) graphite anode electrode before and after cycle tests. Each curve was obtained from (A) a fresh cell and cycled cells with the conditions of (B) 10–70% DOD 25 °C, 2500 cycles, (C) 10–70% DOD 60 °C, 2500 cycles, (D) 0–100% DOD at 25 °C, 2000 cycles and (E) 0–100% DOD 60 °C, 350 cycles.

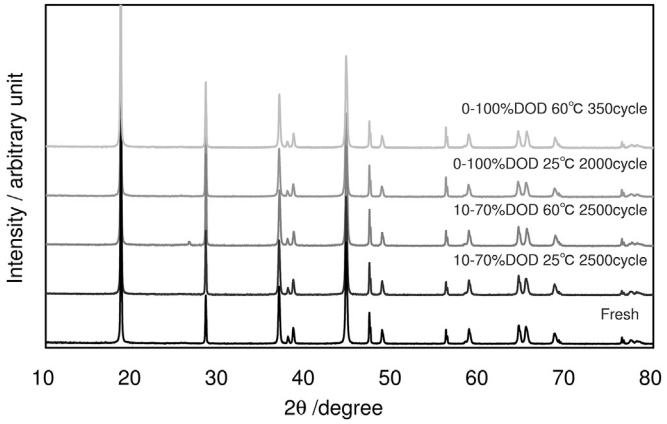

Fig. 4. XRD patterns of the NCA cathode taken out of the model cell (a) before cycle tests, and after cycle tests with the conditions of (b) 10–70% DOD 25 °C, 2500 cycles, (c) 10–70% DOD 60 °C, 2500 cycles, (d) 0–100% DOD 25 °C, 2000 cycles and (e) 0–100% DOD 60 °C, 350 cycles.

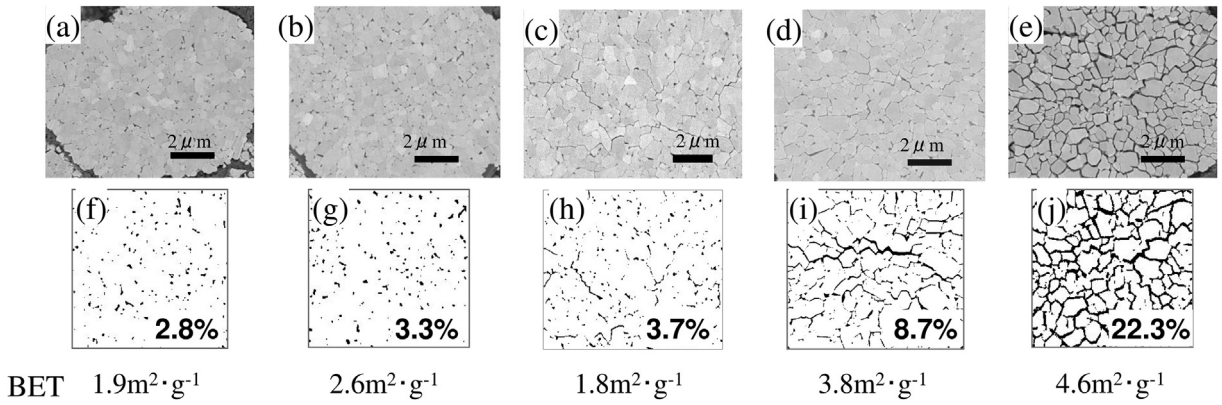

Fig. 5. Cross-sectional SEM images (a–e) and corresponding illustrations in which micro-cracks and pores were drawn in black and NCA was done in white (f–j) for NCA cathode particles (a) before cycle test, and after (b) 10–70% DOD 25 °C, 2500 cycles, (c) 10–70% DOD 60 °C, 2500 cycles, (d) 0–100% DOD 25 °C, 2000 cycles and (e) 0–100% DOD 60 °C, 350 cycles. Inserted numbers in converted images indicate the ratio of area of crack or pore to the BET surface area of cathode electrode.

examined DOD cycle test region more in detail about the influence on the deterioration of the battery.

3.3. Change in morphology and electrochemical properties of $LiAl_yNi_{(1-x-y)}Co_xO_2$ particles with charge–discharge cycling in restricted ΔDODs

A remarkable suppression effect for the micro-crack generation of NCA particles was observed by charge–discharge cycling in the restricted ΔDOD. These phenomena suggested to be because the deterioration occurred in a specific potential range.

In order to verify our hypothesis, charge–discharge cycle tests were performed at 25 °C in four ΔDOD conditions which were 0–60% (4.2–3.54 V), 10–70% (4.05–3.48 V), 40–100% (3.78–2.5 V) and 0–100% as shown in Fig. 6. Fig. 7 shows the change in unit cell volume and lattice parameters of NCA with x value in $Li_{1-x}Al_{0.10}Ni_{0.74}Co_{0.16}O_2$ and DOD. The crystal lattice distortion was observed in range (a) 0–60% (4.2–3.54 V). There was no significant change in unit cell volume and lattice parameters of NCA in range (c) 40–100% (3.78–2.5 V) which was in a specific potential range of deterioration. The capacities were 185 mAh g^{-1} in range (d) 0–100% (4.2 V–2.5 V), it was larger than Ukyo et al. studies [31].

Fig. 8 shows cycle performance of NCA cathode/graphite model cells at 25 °C in four ΔDOD conditions. The capacity fading in the ΔDOD of 0–100% was significantly large compared to that in the other restricted ΔDOD conditions. There was little difference in degradation behavior of discharge capacity among the three restricted ΔDOD conditions. These results suggest that deterioration behavior during cycle tests depends on ΔDOD, does not depend on the lower or upper limit of DOD.

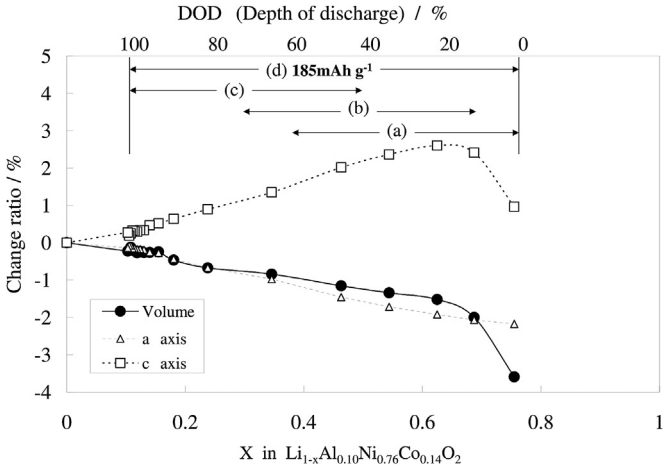

Fig. 7. Change in unit cell volume and lattice parameters of NCA with ΔDOD conditions for charge–discharge cycle tests; (a) 0–60%, (b) 10–70%, (c) 40–100% and (d) 0–100%.

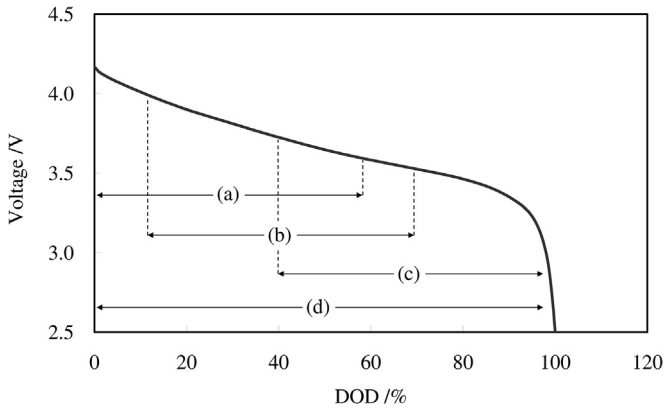

Fig. 6. ΔDOD conditions for charge–discharge cycle tests; (a) 0–60%, (b) 10–70%, (c) 40–100% and (d) 0–100%.

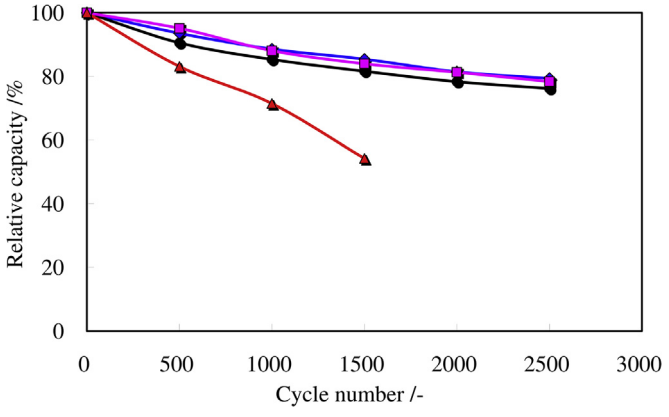

Fig. 8. Cycle performance of model cells under four ΔDOD conditions at 25 °C; (●) 0–60%, (◆) 10–70%, (■) 40–100% and (▲) 0–100%.

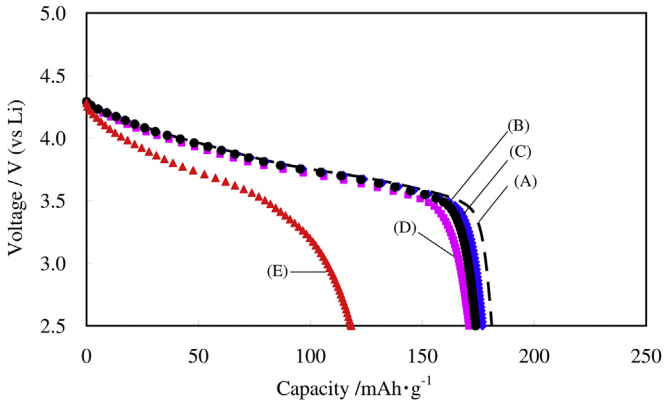

Fig. 9. Discharge curves of (a) NCA cathode electrodes before (A) and after cycle tests under the ΔDOD conditions of (B) 0–60%, (C) 10–70%, (D) 40–100% and (E) 0–100%.

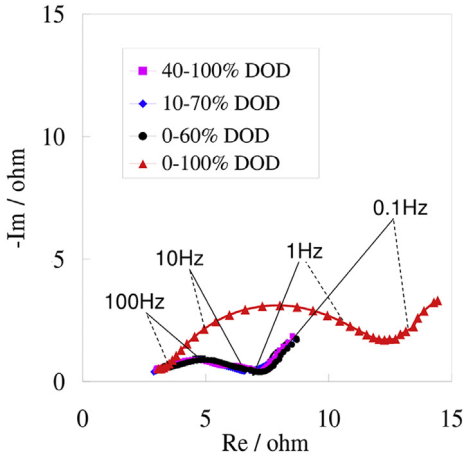

Fig. 10. Nyquist plots of NCA cathode/Li metal coin cells fabricated using NCA cathodes taken out of model cells after cycle tests in the ΔDOD conditions of (●) 0–60%, (◆) 10–70%, (■) 40–100% (after 2500 cycles) and (▲) 0–100% (after 1500 cycles).

In order to investigate why deterioration was accelerated in wider ΔDOD, model cells were disassembled before and after cycle tests and then the cathode and anode electrodes were taken out for analysis. First, the NCA cathode was reassembled into 2016 coin cells with lithium metal electrode as a counter electrode. Fig. 9 shows the discharge curves of the reassembled coin-type cells operated in the voltage region of 4.2–2.5 V for the NCA cathode at a constant current of 0.1C at 25 °C. After 1500 times cycle tests in the ΔDOD of 0–100%, capacity deterioration of the NCA cathode was 35%, while there was no significant deterioration for the other cycle conditions even in after 2500 times cycled.

Change in the impedance of the NCA cathode/Li metal coin-type cells after cycle tests in different ΔDOD conditions was shown in Fig. 10. The cell impedance was measured at 70% DOD at 25 °C. As shown in Fig. 10, the impedance after 2500 times cycled was hardly changed in the ΔDOD conditions of 0–60%, 10–70% and 40–100% which have the ΔDOD of 60%. In contrast, the impedance was greatly increased after the 1500 times cycle in the ΔDOD of 0–100%. These results indicates that the impedance of NCA cathode can maintain stable in each potential region even in cycled 2500 times when the ΔDOD restriction at 60%. The potential range (a) 0–60% (4.2–3.54 V) and (c) 40–100% (3.78–2.5 V) were not in a specific potential range of deterioration.

From the above results, it is obvious that the capacity fading mainly comes from the deterioration of the NCA cathode which was closely dependent upon not upper or lower limit of operation voltage but ΔDOD. Therefore, operations at wider ΔDOD and higher temperature can accelerate cycle life deterioration of the NCA cell.

Fig. 11 shows cross-sectional SEM images of NCA particles before and after cycle tests in the ΔDOD conditions of 0–60%, 10–70% and 40–100% of 2500 cycles and in the ΔDOD of 0–100% of 1500 cycles. As shown in Fig. 11, many micro-cracks were observed after the cycle test in the ΔDOD of 0–100%. In order to quantify micro-crack generation, each SEM image was converted to black areas due to micro-cracks and pores and the other white areas, and then the percentage of black areas was calculated with the same way as Fig. 5. The converted images were displayed in Fig. 11. From the comparison of these images, it was revealed that the micro-crack generation was accelerated in the ΔDOD of 0–100% while it was suppressed in the ΔDOD conditions of 0–60%, 10–70% and 40–100% and there was little difference among three conditions. The results of cross-sectional analysis for range (a) 0–60% (4.2–3.54 V) shows the crystal lattice distortion was not reason of micro-crack generation. These results indicate that this battery can be used up to 4.2 V as upper limit voltage. In the previous studies, the micro-crack was observed at $x = 0.6$ in $Li_{1-x}Al_{0.05}Ni_{0.8}Co_{0.15}O_2$ at initial charge state. Moreover, $Li_{1-x}Al_{0.05}Ni_{0.8}Co_{0.15}O_2$ particles were pulverized after 800cycles [31]. These results were different from results of this investigation. Amine et al. showed that the Al doping suppressed the impedance increase during the aging test [27]. It was thought that the amount of Aluminum and the strength of connection between the NCA primary particles were reason of difference with micro-crack generation. When the DOD value become lower or Li ions are deintercalated from Li sites in NCA, its

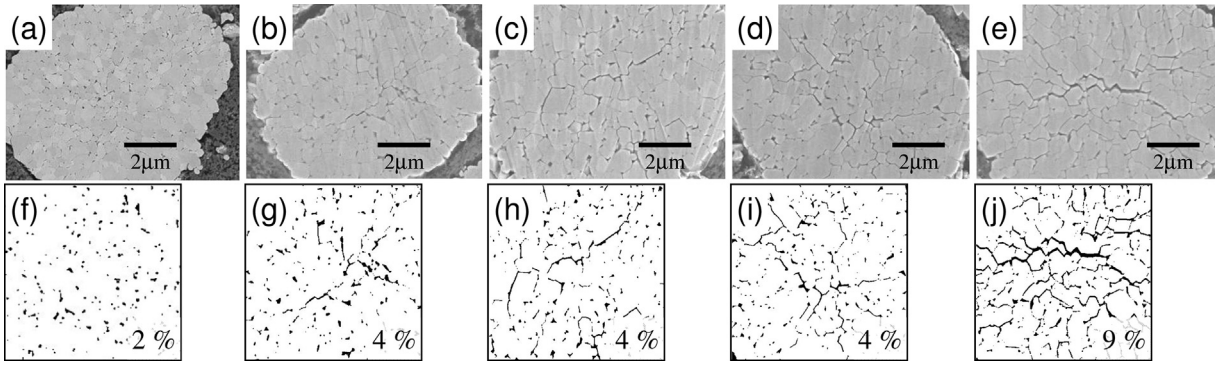

Fig. 11. Cross-sectional SEM images (a–e) and their converted images (f–j) of NCA cathode particles obtained from model cells (a, f) before cycle test, and after cycle test in the ΔDOD conditions of (b, g) 0–60%, (c, h) 10–70%, (d, i) 40–100% of 2500 cycles and (e, j) 0–100% of 1500 cycles. Inserted number in each converted image indicates the percentage of black areas.

unit cells are monotonically contracted and this lasts over the whole DOD range. Therefore it is expected that the larger ΔDOD cause larger volume change of NCA during charge–discharge cycling, which can induce micro-crack generation in NCA particles. Therefore, micro-cracks in NCA particles after cycle test in the ΔDOD of 0–100% are more than those after cycle tests in three restricted ΔDODs whose width is all 60%. Further analysis for surface of micro-crack and deterioration mechanism will be examined in detail in the following literature.

4. Conclusion

In order to verify the mechanism of the cycle life deterioration for NCA cathode LIBs, its capacity fading and the increase in cell resistance for $LiAl_{0.10}Ni_{0.76}Co_{0.14}O_2$ cathode/Graphite anode cylindrical model cells during charge–discharge cycle tests were investigated. The following findings were obtained.

(1) The capacity fading and the increase in cell resistance were dependent upon ΔDOD and test temperature. They were effectively suppressed even in 60 °C when ΔDOD was restricted to 0–60%. On the other hand, large deterioration was observed when ΔDOD was 100% (4.2–2.5 V) especially at high temperature.
(2) The cell deterioration came from not the specific voltage region such as high voltage (4.0–4.2 V) and low voltage (2.5–3.0 V) but the wide region of ΔDOD.
(3) The cell deterioration was caused by the NCA cathode. The change in macro crystal structure of NCA and SEI film growth onto the NCA surface were not observed by XRD and XPS analysis. The micro-crack generation was responsible for the NCA cathode deterioration.

Acknowledgments

This work was supported by the “Li-EAD” program of the New Energy and Industrial Technology Development Organization (NEDO), (07002679-0). The authors express their thanks to members of Lithium ion Battery Business Unit (A. Nagasaki, N. Yamamoto and H. Kaiya) and Prof. Hiroshi Inoue in Osaka Prefecture University.

References

[1] N. Yamamoto, K. Nakura, S. Yuasa, T. Kurosaki, Panasonic Tech. J. 56 (2010) 2.
[2] T. Ohzuku, A. Ueda, M. Nagayama, J. Electrochem. Soc. 140 (1993) 1862.
[3] T. Ohzuku, A. Ueda, M. Kouguchi, J. Electrochem. Soc. 142 (1995) 4033.
[4] H. Arai, S. Okada, Y. Sakurai, J. Yamaki, J. Electrochem. Soc. 144 (1997) 3117.
[5] C. Delmas, M. Ménétrier, L. Croguennec, I. Saadoune, A. Rougier, C. Pouillerie, G. Prado, M. Grüne, L. Fournès, Electrochim. Acta 45 (1999) 243.
[6] H. Arai, M. Tsuda, Y. Sakurai, J. Power Sources 90 (2000) 76.
[7] A.N. Mansour, X.Q. Yang, X. Sun, J. McBreen, L. Croguennec, C. Delmas, J. Electrochem. Soc. 147 (2000) 2104.
[8] G. Prado, A. Rougier, L. Fournes, C. Delmas, J. Electrochem. Soc. 147 (2000) 2880.
[9] K.K. Lee, W.S. Yoon, K.B. Kim, K.Y. Lee, S.T. Hong, J. Power Sources 97 (2001) 308.
[10] A. Kinoshita, K. Yanagida, A. Yanai, Y. Kida, A. Funahashi, T. Nohma, I. Yonezu, J. Power Sources 102 (2001) 283.
[11] P. Biensan, J.P. Pérès, F. Perton, in: Abstract of the ECS Fall Meeting, Hawaii, 1999. Abstract #131.
[12] C.H. Chen, J. Liu, K. Amine, in: Abstract of the ECS Fall Meeting, San Francisco, 2001. Abstract #176.
[13] S. Madhavi, G.V.S. Rao, B.V.R. Chowdari, S.F.Y. Li, J. Power Sources 93 (2001) 156.
[14] S. Albrecht, J. Kümpers, M. Kruft, S. Malcus, C. Vogler, M. Wahl, M. Wohlhart-Mehrens, J. Power Sources 119-121 (2003) 178.
[15] M. Broussely, S. Herreyre, P. Biensan, P. Kasztejna, K. Nechev, R.J. Staniewicz, J. Power Sources 97 (2001) 13.
[16] M. Broussely, P. Blanchard, P. Biensan, J.P. Planchat, K. Nechev, R.J. Staniewicz, J. Power Sources 119 (2003) 859.
[17] M. Broussely, P. Biensan, F. Bonhomme, P. Blanchard, S. Herreyre, K. Nechev, R.J. Staniewicz, J. Power Sources 146 (2005) 90.
[18] S. Watanabe, K. Nakura, in: Abstract of the ABAA, Tokyo, 2009. Abstract #13.
[19] S. Watanabe, M. Kinoshita, K. Nakura, J. Power Sources 196 (2011) 6906.
[20] C.H. Chen, J. Liu, K. Amine, J. Power Sources 96 (2001) 321.
[21] K. Amine, C.H. Chen, J. Liu, M.H. Hammond, A. Jansen, D. Dees, I. Bloom, D. Vissers, G. Henriksen, J. Power Sources 97-98 (2001) 684.
[22] I. Bloom, B.W. Cole, J.J. Sohn, S.A. Jones, E.G. Polzin, V.S. Battaglia, G.L. Henriksen, C. Motloch, R. Richardson, T. Unkelhaeuser, D. Ingersoll, H.L. Case, J. Power Sources 101 (2001) 238.
[23] I. Bloom, S.A. Jones, V.S. Battaglia, G.L. Henriksen, J.P. Christophersen, R.B. Wright, C.D. Ho, J.R. Belt, C.G. Motloch, J. Power Sources 124 (2003) 538.
[24] R.B. Wright, C.G. Motloch, J.R. Belt, J.P. Christophersen, C.D. Ho, R.A. Richardson, I. Bloom, S.A. Jones, V.S. Battaglia, G.L. Henriksen, T. Unkelhaeuser, D. Ingersoll, H.L. Case, S.A. Rogers, R.A. Sutula, J. Power Sources 110 (2002) 445.
[25] J. Shim, R. Kostecki, T. Richardson, X. Song, K.A. Striebel, J. Power Sources 112 (2002) 222.
[26] R.G. Jungst, G. Nagasubramanian, H.L. Case, B.Y. Liaw, A. Urbina, T.L. Paez, D.H. Doughty, J. Power Sources 119–121 (2003) 870.
[27] C.H. Chen, J. Liu, M.E. Stoll, G. Henriksen, D.R. Vissers, K. Amine, J. Power Sources 128 (2004) 278.
[28] D.P. Abraham, J.L. Knuth, D.W. Dees, I. Bloom, J.P. Christophersen, J. Power Sources 170 (2007) 465.
[29] Y. Zhang, C.Y. Wang, J. Electrochem. Soc. 156 (2009) A527.
[30] K.A. Striebel, J. Shim, E.J. Cairns, R. Kostecki, Y.-J. Lee, J. Reimer, T.J. Richardson, P.N. Ross, X. Song, G.V. Zhuang, J. Electrochem. Soc. 151 (2004) A857.
[31] Y. Itou, Y. Ukyo, J. Power Sources 146 (2005) 39.
[32] S. Muto, Y. Sasano, K. Tatsumi, T. Sasaki, K. Horibuchi, Y. Takeuchi, Y. Ukyo, J. Electrochem. Soc. 156 (2009) A371.
[33] S. Zheng, R. Huang, Y. Makimura, Y. Ukyo, C.A.J. Fisher, T. Hirayama, Y. Ikuhara, J. Electrochem. Soc. 158 (2011) A357.
[34] Y. Makimura, S. Zheng, Y. Ikuhara, Y. Ukyo, J. Electrochem. Soc. 159 (2012) A1070.
[35] S. Watanabe, M. Kinoshita, K. Nakura, in: Abstract of the IMLB Meeting, Montréal, 2010.
[36] S. Watanabe, T. Hosokawa, K. Morigaki, M. Kinoshita, K. Nakura, ECS Trans. 41 (2012) 65.